

# TrkB kinase activity maintains synaptic function and structural integrity at adult neuromuscular junctions

Carlos B. Mantilla,<sup>1,2</sup> Jessica M. Stowe,<sup>1</sup> Dylan C. Sieck,<sup>1</sup> Leonid G. Ermilov,<sup>1</sup> Sarah M. Greising,<sup>1</sup> Chao Zhang,<sup>3</sup> Kevan M. Shokat,<sup>3</sup> and Gary C. Sieck<sup>1,2</sup>

<sup>1</sup>Department of Physiology and Biomedical Engineering, Mayo Clinic College of Medicine, Rochester, Minnesota;

<sup>2</sup>Department of Anesthesiology, Mayo Clinic College of Medicine, Rochester, Minnesota; and <sup>3</sup>Cellular and Molecular Pharmacology, University of California, San Francisco, San Francisco, California

Submitted 27 December 2013; accepted in final form 14 August 2014

**Mantilla CB, Stowe JM, Sieck DC, Ermilov LG, Greising SM, Zhang C, Shokat KM, Sieck GC.** TrkB kinase activity maintains synaptic function and structural integrity at adult neuromuscular junctions. *J Appl Physiol* 117: 910–920, 2014. First published August 28, 2014; doi:10.1152/jappphysiol.01386.2013.—Activation of the tropomyosin-related kinase receptor B (TrkB) by brain-derived neurotrophic factor acutely regulates synaptic transmission at adult neuromuscular junctions (NMJs). The role of TrkB kinase activity in the maintenance of NMJ function and structure at diaphragm muscle NMJs was explored using a chemical-genetic approach that permits reversible inactivation of TrkB kinase activity in *TrkB<sup>F616A</sup>* mice by 1NMPP1. Inhibiting TrkB kinase activity for 7 days resulted in significant, yet reversible, impairments in neuromuscular transmission at diaphragm NMJs. Neuromuscular transmission failure following 2 min of repetitive phrenic nerve stimulation increased from 42% in control to 59% in 1NMPP1-treated *TrkB<sup>F616A</sup>* mice ( $P = 0.010$ ). Recovery of TrkB kinase activity following withdrawal of 1NMPP1 treatment improved neuromuscular transmission ( $P = 0.006$ ). Electrophysiological measurements at individual diaphragm NMJs documented lack of differences in quantal content in control and 1NMPP1-treated mice ( $P = 0.845$ ). Morphological changes at diaphragm NMJs were modest following inhibition and recovery of TrkB kinase activity. Three-dimensional reconstructions of diaphragm NMJs revealed no differences in volume at motor end plates (labeled by  $\alpha$ -bungarotoxin;  $P = 0.982$ ) or presynaptic terminals (labeled by synaptophysin;  $P = 0.515$ ). Inhibition of TrkB kinase activity by 1NMPP1 resulted in more compact NMJs, with increased apposition of presynaptic terminals and motor end plates ( $P = 0.017$ ) and reduced fragmentation of motor end plates ( $P = 0.005$ ). Recovery of TrkB kinase activity following withdrawal of 1NMPP1 treatment resulted in postsynaptic remodeling likely reflecting increased gutter depth ( $P = 0.007$ ), without significant presynaptic changes. These results support an essential role for TrkB kinase activity in maintaining synaptic function and structural integrity at NMJs in the adult mouse diaphragm muscle.

diaphragm muscle; innervation; motor unit; neuromuscular transmission; synaptic plasticity

NEUROTROPHINS, signaling via their high-affinity tropomyosin-related kinase (Trk) receptors, are important regulators of synaptic plasticity and function at the neuromuscular junction (NMJ) (12, 29). Both brain-derived neurotrophic factor (BDNF) (23) and neurotrophin-4 (NT-4) (52), acting via Trk subtype B (TrkB) receptors, increase spontaneous and evoked neurotransmitter release in cultured amphibian NMJs. In rodents, BDNF, NT-4, and the novel TrkB ligand 7,8-dihydroflavone prevent force loss associated with repetitive nerve

stimulation (25, 30), reflecting improved neuromuscular transmission. Signaling via TrkB receptors modulates neurotransmitter release by interacting with presynaptic muscarinic receptors (14). In addition, BDNF-induced TrkB signaling contributes to the stabilization of polyinnervated NMJs during the postnatal period of synaptic elimination (13). In adult mice, fragmentation of postsynaptic acetylcholine receptor (AChR) clusters is induced via adenovirus-mediated overexpression of truncated TrkB (TrkB.t1) (15), likely reflecting reduced full-length TrkB signaling (kinase activity). In general agreement, postsynaptic terminal expansion and fragmentation are evident in *TrkB<sup>+/-</sup>* mice with reduced expression of the full-length TrkB receptor (22). Genetic knockdown models lacking TrkB receptors or BDNF die during embryonic or early postnatal development (50), and heterozygous models with reduced expression do not avoid possible developmental effects on NMJ function and structure. The role that TrkB kinase activity plays in the maintenance of functional and structural properties of the adult NMJ in vivo has not been explored in developmentally intact mice, and thus developmental effects of altered TrkB signaling cannot be obviated when studying adult knock-out mice.

The purpose of the present study was to examine the role of TrkB kinase activity on the maintenance of synaptic function and structural integrity at diaphragm muscle NMJs in adult mice using a chemical-genetic approach in *TrkB<sup>F616A</sup>* mice expressing knockin alleles that permit rapid, selective, and reversible inhibition of TrkB kinase activity (6). *TrkB<sup>F616A</sup>* knockin mice carry a phenylalanine-to-alanine mutation in the ATP binding domain of the TrkB receptor, rendering TrkB kinase activity sensitive to inhibition by the phosphoprotein phosphatase 1 inhibitor (PPI) derivative 1NMPP1. Thus this chemical-genetic approach permits assessment of the in vivo role of TrkB kinase activity in the regulation of neuromuscular transmission and maintenance of morphological properties at adult diaphragm NMJs.

## MATERIALS AND METHODS

**Animals.** The study was approved by the Institutional Animal Care and Use Committee (IACUC), and all procedures were performed in accordance with the American Physiological Society's *Guiding Principles in the Care and Use of Vertebrate Animals in Research and Training*. Adult male *TrkB<sup>F616A</sup>* mice ( $n = 58$ ;  $24.9 \pm 0.3$  g) were used to selectively, rapidly, and reversibly inhibit TrkB kinase activity following oral 1NMPP1 treatment (25  $\mu$ M in drinking water). All mice were individually housed and maintained on a 12:12-h light-dark schedule under specific pathogen-free conditions with ad libitum access to food and water. While undergoing oral 1NMPP1 treatment water intake was monitored daily. *TrkB<sup>F616A</sup>* mice were generated on

Address for reprint requests and other correspondence: C. B. Mantilla, Depts. of Physiology and Biomedical Engineering and of Anesthesiology, 200 First St., SW, Rochester, MN 55905 (e-mail: mantilla.carlos@mayo.edu).

a 129J and C57BL/6 hybrid genetic background and were genetically modified to stably harbor a knockin mutation that results in inhibition of TrkB kinase activity only in the presence of PP1 derivatives such as 1NMPP1 (6). 1NMPP1 was synthesized as previously described (3). Three groups were studied: 1) untreated mice (age- and weight-matched; CTL;  $n = 23$ ); 2) mice in which TrkB kinase activity was inhibited by treatment with 1NMPP1 for 7 days (INH;  $n = 23$ ); and 3) mice in which TrkB kinase activity was reversibly inhibited by treatment with 1NMPP1 for 7 days followed by a 7-day recovery period (REC;  $n = 12$ ). These time points were based on previous studies demonstrating substantial functional and morphological changes at diaphragm NMJs following 7–14 days of altered synaptic activity (27, 28, 38, 48, 49). At the terminal experiment, animals were exsanguinated under deep levels of anesthesia induced by intramuscular injection of ketamine (90 mg/kg) and xylazine (10 mg/kg).

**Assessment of neuromuscular transmission failure.** Isolated diaphragm muscle-phrenic nerve preparations from mice in all three experimental groups ( $n = 6$ –7/group) were used to determine neuromuscular transmission failure, using a global measurement as previously described (10, 11, 18, 21, 25, 30, 33, 38, 45). Briefly, muscle segments (2- to 3-mm wide) were obtained from each midcostal hemidiaphragm muscle while preserving the phrenic nerves. Segments were placed in an organ bath containing oxygenated (95% O<sub>2</sub>-5% CO<sub>2</sub>) Rees-Simpson solution (in mM: 135 Na<sup>+</sup>, 5 K<sup>+</sup>, 2 Ca<sup>2+</sup>, 1 Mg<sup>2+</sup>, 120 Cl<sup>-</sup>, 25 HCO<sub>3</sub><sup>-</sup>, 11 glucose; pH 7.4) at 26°C, and isometric diaphragm muscle force measurements were obtained by attaching the central tendon to a force transducer (model 6350, Cambridge Technology, Cambridge, MA) and the rib insertion to a micromanipulator. Direct muscle stimulation (1-ms pulses via plate electrodes) was used to adjust muscle length until maximal isometric twitch force responses were obtained (optimal length:  $L_0$ ). The phrenic nerve was subsequently stimulated (0.2-ms pulse at supra-maximal intensity) using a suction electrode at 40 Hz in 330-ms duration trains repeated each second for a 2-min period. Every 15 s, direct muscle stimulation (via plate electrodes; 1-ms supramaximal pulses at 40 Hz in 330-ms trains) was superimposed (Fig. 1A). The evoked isometric force responses were displayed on a storage oscilloscope and recorded with customized software (LabView 8.2, National Instruments, Austin, TX) running on a personal computer. In every diaphragm muscle-phrenic nerve preparation, care was taken to ensure that the initial forces generated by both nerve and muscle stimulation were within expected ranges consistent with previous studies (10, 11, 18, 21, 25, 30, 32, 38, 45). The extent of transmission failure was estimated based on the difference in force generated by nerve vs. muscle stimulation as  $(NF - MF)/(1 - MF)$ , where NF and MF are the percent decrement in force during repetitive nerve and muscle stimulation, respectively.

In separate diaphragm muscle segments, contractile properties were also assessed. Isometric twitch force ( $P_t$ ) and maximum tetanic force ( $P_o$ ) were normalized for cross-sectional area based on muscle weight and a tissue density of 1.056 g/cm<sup>3</sup> at optimal muscle length ( $L_0$ ). In addition, the ratio of force generated after 2 min of repetitive stimulation (330 ms, 40-Hz trains) to the initial force was used to determine a muscle fatigue index.

**Electrophysiological assessment of quantal content.** In an additional set of experiments, diaphragm muscle preparations with the phrenic nerve attached were dissected from mice in the CTL and INH groups to determine miniature and evoked end-plate potentials (mEPP and EPP, respectively) using standard methods for electrophysiological recordings, as previously described (9, 11, 43). Briefly, preparations were pinned to a silicon rubber-coated dish containing Rees-Simpson solution. A recording glass micropipette filled with 3 M KCl (15–20 M $\Omega$ ) was inserted at the edge of selected superficial presynaptic terminals into the corresponding muscle fiber. Visualization of the terminals was accomplished with the use of a Photometrics Cascade:512F cooled charge-couple device camera (Photometrics-Roper Scientific, Tucson, AZ) mounted on an upright Olympus

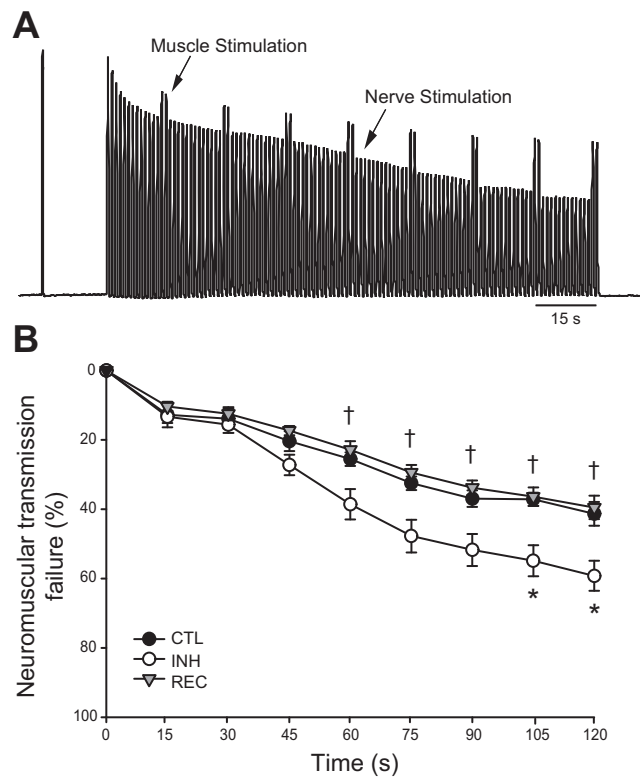


Fig. 1. Contribution of neuromuscular transmission failure to muscle fatigue in diaphragm muscle from adult *TrkB<sup>F616A</sup>* mice in control (CTL), 1NMPP1-inhibited (INH), and recovered (REC) experimental groups. **A:** representative tracing of force elicited by stimulation of the diaphragm muscle via the phrenic nerve (every s) and muscle stimulation via plate electrodes (every 15 s). Maximal isometric twitch force obtained by direct muscle stimulation is shown by the first spike. Muscle fatigue induced by repetitive stimulation is evident by the decrease in force over time. The difference in the force elicited by direct (muscle) and indirect (nerve) stimulation reflects neuromuscular transmission failure, which was quantified as described in MATERIALS AND METHODS. **B:** the global measure of neuromuscular transmission failure represents the percent neuromuscular transmission failure with an inverted y-axis (i.e., greater % neuromuscular transmission failure reflects impaired force generation elicited by nerve stimulation). Time course (mean  $\pm$  SE) of neuromuscular transmission failure in CTL ( $n = 7$ ), INH ( $n = 7$ ) and REC ( $n = 6$ ) mice. Neuromuscular transmission failure after 2 min of repetitive stimulation is significantly greater in the INH group compared with CTL and REC (ANOVA,  $P = 0.003$ ). \*Significantly different from CTL group ( $P < 0.05$ ). †Significantly different from INH group ( $P < 0.05$ ).

BX51WI microscope, with the use of a Huxley MP-85 micromanipulator (Sutter Instruments, Novato, CA). Muscle contractions were blocked with  $\mu$ -conotoxin GIIIb (15.8  $\mu$ g/ml, 6  $\mu$ M; Bachem). Supramaximal electrical stimulation of the phrenic nerves (10–20 V, 0.1 ms) was delivered using a Grass S88 stimulator (Grass Instruments). Resting membrane potential, miniature end-plate potentials (mEPP), and end-plate potentials (EPP) in response to isolated, single phrenic nerve stimulation were recorded using a Duo 773 electrometer (World Precision Instruments, Sarasota, FL) and analog-to-digital converted using a Digidata 1322A interface (Axon Instruments) using AxoScope 10.4 software (Axon Instruments). Only muscle fibers with stable resting membrane potential in excess of  $-60$  mV ( $<5\%$  fluctuation) were used. Quantal content was estimated as the ratio of EPP amplitude corrected for nonlinear summation (31), and mean mEPP amplitude. Data were examined offline using Clampfit 10.4 software (Axon Instruments).

**Assessment of diaphragm muscle NMJ morphology.** Morphological assessments of pre- and postsynaptic structures were conducted in

mice from all three experimental groups ( $n = 5\text{--}6/\text{group}$ ). The diaphragm muscle was quickly excised and pinned onto a silicon rubber (Sylgard; Dow-Corning, Midland, MI)-coated Petri dish. The motor end plate of diaphragm NMJs was labeled by incubating in Alexa Fluor 488-conjugated  $\alpha$ -bungarotoxin ( $0.1 \mu\text{g}/\text{ml}$ ; Invitrogen, Carlsbad, CA) for 45 min. Subsequently, diaphragm muscle samples were washed with  $0.1 \text{ M}$  phosphate buffer, fixed with 4% paraformaldehyde, washed, and stained for presynaptic structures overnight using  $1 \text{ mg}/\text{ml}$  of an anti-synaptophysin antibody (SC-9116, Santa Cruz Biotechnology, Santa Cruz, CA) and the appropriate Cy3-conjugated secondary antibody (donkey anti-rabbit IgG, Jackson Immuno Research Laboratories, West Grove, PA). Additional studies not including  $\alpha$ -bungarotoxin or the primary anti-synaptophysin antibody (blank) or alternately using a Cy5-conjugated secondary antibody were conducted to confirm the specificity of immunostaining. Blank sections were processed in parallel for all immunohistochemical reactions and animals.

**Assessment of antibody specificity.** The specificity of fluorescently-conjugated  $\alpha$ -bungarotoxin labeling was confirmed by the absence of staining outside of motor end plates in the diaphragm and other skeletal muscles in mice and rats, as previously reported (26, 27, 37, 38, 43, 45). For identification of presynaptic structures at diaphragm NMJs, we selected an anti-synaptophysin antibody that specifically recognizes a region between amino acids 269 and 289 (19) in the cytoplasmic domain of this integral membrane glycoprotein ( $\sim 40 \text{ kDa}$ ) (53). The antiserum stains a single band of  $38\text{-kDa}$  molecular mass on Western blot (manufacturer's technical information). The immunoreactivity pattern observed was identical to previous reports of axon terminals in rat diaphragm muscle (26, 27, 38, 43). Antibodies anti-TrkB (Neuromics no. GT15080) and anti-pTrkB (Cell Signaling no. 4621S) stain band(s) of the appropriate molecular weight (verified in Western blot analysis of brain extracts).

**Confocal imaging.** Confocal microscopy was used for morphological analyses of diaphragm muscle NMJs, as previously described (27, 40, 41, 45, 46, 48). Diaphragm muscle whole mounts were imaged with an Olympus Fluoview 300 laser scanning confocal microscope (Olympus America, Melville, NY) mounted on an upright Olympus BX50WI microscope and equipped with Argon (488 nm) and HeNe (543 nm and 643 nm) lasers using an Olympus LUMPlanFl 60 $\times$ 0.90 N.A. water immersion lens. Pixel dimensions ( $0.33 \times 0.33 \mu\text{m}$  in a  $800 \times 600$  array) were set above the optical resolution for this lens and step size was set to match the empirically determined Z-axis resolution ( $0.8 \mu\text{m}$ ), thus avoiding oversampling (26, 27, 45). During imaging and subsequent analyses, technicians were unaware of experimental group assignment. Confocal image stacks were obtained for all NMJs that were en face and located superficially on the thoracic surface of the diaphragm muscle (within  $50 \mu\text{m}$ ), as in previous studies (26, 27, 38, 45).

Stacks of confocal images (2-channel, 12-bit multi-TIFF files) for each diaphragm muscle NMJ were used for morphometric measurements of pre- and postsynaptic structures (in MetaMorph, Molecular Devices, Sunnyvale, CA). A postsynaptic 2D planar area (motor end plate) was obtained from a maximum-intensity projection, and the relative planar area was calculated by dividing the 2D planar area by the area described by the main orthogonal axes of the end plate. The relative planar area thus reflects the complexity of postsynaptic structures as determined by branching and fragmentation of the motor end plate (45). The volume of the presynaptic terminal, motor end plate and volume of apposition of pre- and postsynaptic structures were also determined with manual thresholding using a customized algorithm in MetaMorph, as previously reported (38, 45). The volume of apposition was determined from the intersection of the two binarized volume sets for pre- and postsynaptic structures. Previous investigations commonly assess apposition of pre- and postsynaptic structures using 2D analyses of maximum-intensity projections (22, 38). The density of AChR at the NMJ was estimated by average fluorescence intensity of Alexa Fluor 488-conjugated  $\alpha$ -bungarotoxin.

In preliminary studies, a subset of 22 CTL NMJs was analyzed comparing 2D and 3D measurements of pre- and postsynaptic apposition. Using binarized 2D maximum-intensity projections of presynaptic terminals and motor end plates, the average fraction of the presynaptic terminal directly opposing postsynaptic structures was  $88.8 \pm 1.5\%$ . In addition,  $75.0 \pm 1.2\%$  of the motor end plate was directly opposed by the presynaptic terminal. These findings are consistent with previous reports, including measurements at type-identified diaphragm NMJs (37–39, 42). However, 3D measurements of the same NMJs showed that, on average,  $59.4 \pm 3.9\%$  of the presynaptic terminal volume was opposing the motor end plate and  $53.5 \pm 2.5\%$  of the motor end-plate volume was directly opposed by the corresponding presynaptic terminal. Furthermore, these analyses revealed that 2D measurements of apposition would frequently overestimate apposition by up to 40%. For this reason, only 3D volumetric measurements of pre- and postsynaptic apposition are reported in this study.

Images for publication were produced in Adobe Photoshop (Adobe Systems; San Jose, CA) by down-converting multi-TIFF files to 8-bit single-channel images, without introducing any changes in brightness or contrast.

**Statistical analysis.** All statistical evaluations were performed using standard statistical software (JMP 8.0, SAS Institute, Cary, NC). Data are reported as means  $\pm$  SE, unless otherwise specified. Comparisons of neuromuscular transmission failure were conducted using repeated-measures ANOVA. Morphological and electrophysiological data were clustered by animal such that all measurements represent mean values across animals for each experimental group; differences were compared using one-way ANOVA. When appropriate, post hoc group differences were assessed using the Tukey-Kramer honestly significant difference (HSD) test. A value of  $P < 0.05$  was considered statistically significant.

## RESULTS

**Inhibition of TrkB kinase activity.** To measure the effects of inhibiting TrkB kinase activity *in vivo*, 1NMPP1 was administered orally to *TrkB<sup>F616A</sup>* mice for 7 days. Adult *TrkB<sup>F616A</sup>* mice that were administered 1NMPP1 did not show any gross abnormalities. Animals gained weight normally during the 7-day inhibitor treatment. No overt changes were observed in animal behavior or motor function during the treatment period, nor during recovery from inhibition, compared with CTL. Inhibition of TrkB kinase activity was verified in protein extracted from brain tissue, immunoprecipitated using anti-TrkB, and probed for phosphorylated TrkB. Treatment with 1NMPP1 in *TrkB<sup>F616A</sup>* mice resulted in extensive reduction in phosphorylated TrkB, with the ratio of phosphorylated to total TrkB being reduced  $\sim 13$ -fold ( $P < 0.05$ ). Assessment of 1NMPP1-induced changes in TrkB phosphorylation was not possible in diaphragm muscle homogenates from CTL mice, given very low levels of full-length TrkB and undetectable phosphorylated TrkB precluding quantitative assessment.

**TrkB kinase inhibition increases neuromuscular transmission failure.** To evaluate possible effects induced by altered TrkB kinase activity on neuromuscular transmission, diaphragm muscle segments with the phrenic nerve attached were stimulated *in vitro*. A representative tracing of diaphragm muscle forces elicited by independent phrenic nerve and muscle stimulation is shown in Fig. 1. With repetitive stimulation, forces elicited in response to nerve stimulation decline more rapidly than those elicited in response to muscle stimulation, reflecting an increasing contribution of neuromuscular transmission failure to reduced force generation (Fig. 1A). Neuromuscular trans-

mission failure determined in this fashion is a global method to evaluate force generated by the diaphragm muscle in response to nerve activation. These findings are consistent with previous reports in the mouse diaphragm from wild-type (45) and *TrkB<sup>F616A</sup>* mice (25).

The effect on neuromuscular transmission failure elicited by repetitive stimulation in vitro was determined in diaphragm muscle segments obtained from adult CTL, INH, and REC *TrkB<sup>F616A</sup>* mice. In vitro conditions were identical for all three groups; e.g., 1NMPP1 was not present in the bath solution during testing in the INH group. The ratio of initial force generated by nerve stimulation to that generated by muscle stimulation did not differ across the experimental groups (overall:  $0.84 \pm 0.01$ ;  $P > 0.05$ ).

There were significant differences in neuromuscular transmission failure following 2 min of repetitive nerve stimulation across the three experimental groups [ANOVA;  $F(2,17) = 8$ ,  $P = 0.003$ ]. Following 7 days of 1NMPP1-induced inhibition of TrkB kinase activity, neuromuscular transmission was significantly impaired compared with CTL, and this effect was evident after 105 s of repetitive stimulation [Fig. 1B; repeated-measures ANOVA;  $F(16,136) = 4.12$ ,  $P < 0.001$ ]. Indeed, by 2 min of repetitive nerve stimulation, neuromuscular transmission failure was greater in the INH group compared with CTL (CTL  $41.6 \pm 4.0\%$  vs. INH  $58.9 \pm 3.7\%$ ; post hoc HSD test,  $P = 0.010$ ). These results indicate that inhibition of TrkB kinase activity in vivo disrupts neuromuscular transmission.

Of note, inhibition of TrkB kinase activity by 1NMPP1 in *TrkB<sup>F616A</sup>* mice did not affect isometric contractile properties of the diaphragm muscle [Table 1; ANOVA:  $P_t$ ,  $F(2,21) = 0.3$ ,  $P = 0.730$ ;  $P_o$ ,  $F(2,21) = 0.2$ ,  $P = 0.834$ ; and fatigue index,  $F(2,17) = 0.7$ ,  $P = 0.529$ ]. Compared with CTL, there were no differences in specific muscle force ( $P_t$  and  $P_o$ ; post hoc HSD test,  $P = 0.820$  and  $P = 0.853$ , respectively) or in the relative force generated by the diaphragm muscle following 2 min of repetitive stimulation (i.e., fatigue index; post hoc HSD test,  $P = 0.978$ ).

*Neuromuscular transmission is restored with recovery from TrkB kinase inhibition.* To determine whether altered functional properties induced by inhibition of TrkB kinase activity were reversible, adult male *TrkB<sup>F616A</sup>* mice that were initially treated with 1NMPP1 for 7 days (as in the INH group) were now allowed to recover from 1NMPP1-induced inhibition by withdrawal of 1NMPP1 treatment. Following 7 days of recovery without the inhibitor 1NMPP1, neuromuscular transmission was significantly improved compared with INH (Fig. 1B),

Table 1. Isometric contractile and fatigue properties of diaphragm muscle segments in *TrkB<sup>F616A</sup>* mice

	$P_t$ , N/cm <sup>2</sup>	$P_o$ , N/cm <sup>2</sup>	Fatigue Index, %
Control <i>TrkB<sup>F616A</sup></i> (CTL)	$6.8 \pm 0.3$ (10)	$20.5 \pm 0.7$ (10)	$40.1 \pm 2.3$ (7)
1NMPP1 inhibited (INH)	$6.4 \pm 0.6$ (8)	$19.9 \pm 1.2$ (8)	$39.4 \pm 3.4$ (7)
Recovered (REC)	$6.9 \pm 0.5$ (6)	$19.9 \pm 0.6$ (6)	$43.7 \pm 2.2$ (6)

Data are presented as means  $\pm$  SE and, in parentheses, number of animals for each measurement.  $P_t$ , peak isometric twitch force;  $P_o$ , maximum tetanic force [both normalized for physiological cross-sectional area (i.e., specific force)]. Fatigue index is the relative force elicited following 2 min of repetitive stimulation as a percentage of the initial force from a midcostal diaphragm muscle segment separate from that used for neuromuscular transmission analysis. All comparisons conducted using a one-way ANOVA were not significant ( $P > 0.05$ ).

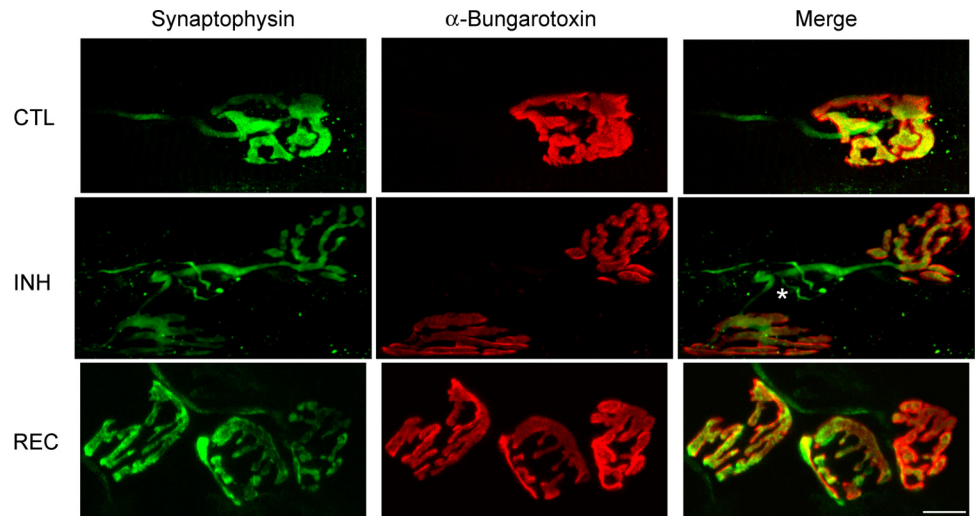
and this effect was evident after 60 s of repetitive stimulation [repeated-measures ANOVA,  $F(16,136) = 4.12$ ,  $P < 0.001$ ]. By 2 min of repetitive nerve stimulation, neuromuscular transmission failure was significantly decreased in the REC group ( $39.5 \pm 3.4\%$ ) compared with INH (post hoc HSD test,  $P = 0.006$ ). Furthermore, no differences in neuromuscular transmission failure were observed between the REC and CTL groups following 2 min of repetitive phrenic nerve stimulation (post hoc HSD test,  $P = 0.917$ ). Thus functional changes at diaphragm NMJs were reversible following recovery from 1NMPP1-induced inhibition of TrkB kinase activity in *TrkB<sup>F616A</sup>* mice.

Consistent with the lack of effect of 1NMPP1-induced inhibition of TrkB kinase activity on contractile properties of the diaphragm muscle, there were no differences in contractile properties following recovery from 1NMPP1-induced inhibition of TrkB kinase activity [Table 1; ANOVA:  $P_t$ ,  $F(2,21) = 0.3$ ,  $P = 0.730$ ;  $P_o$ ,  $F(2,21) = 0.2$ ,  $P = 0.834$ ; and fatigue index,  $F(2,17) = 0.7$ ,  $P = 0.529$ ]. Compared with INH or CTL, there were no differences in specific muscle force ( $P_t$  and  $P_o$ ; post hoc HSD test,  $P = 0.735$  and  $P = 0.999$ , respectively, vs. INH) or in the relative force generated by the diaphragm muscle following 2 min of repetitive stimulation (i.e., fatigue index; post hoc HSD test,  $P = 0.533$  vs. INH).

*TrkB kinase inhibition results in modest morphological changes at diaphragm NMJs.* Morphological analyses of diaphragm muscle NMJs were conducted using confocal imaging of en face fluorescently-labeled NMJs to determine whether changes in diaphragm NMJ function were associated with corresponding changes in NMJ structure. Excellent labeling of motor end plates using  $\alpha$ -bungarotoxin was evident in all diaphragm muscle preparations. Immunoreactivity to the synaptic vesicle protein synaptophysin labeled presynaptic terminals and axons in all experimental groups. Figure 2 displays representative maximum-intensity projections for pre- and postsynaptic structures of diaphragm NMJs from CTL, INH, and REC *TrkB<sup>F616A</sup>* mice. Following 1NMPP1 treatment, some individual NMJs displayed reorganization of presynaptic terminals and disruption of motor axons (Fig. 2). This type of axon terminal ending was not evident in the diaphragm muscle from CTL mice. However, a detailed analysis of motor axon branching is not possible using synaptophysin labeling. Importantly, all visualized NMJs displayed both pre- and postsynaptic structures, suggesting lack of synaptic denervation following inhibition of TrkB kinase activity.

To measure gross changes in NMJ structure, motor end-plate area and an index of NMJ complexity were first obtained from maximum-intensity projections for each NMJ. On average, 37 NMJs were analyzed per animal with a total of 662 NMJs across the three experimental groups. Although diaphragm NMJ planar area (2D) differed across the experimental groups [ANOVA;  $F(2,15) = 4$ ,  $P = 0.042$ ], pairwise post hoc comparisons (HSD test) did not achieve statistical significance. Specifically, planar area (2D) of diaphragm NMJs was not significantly different following 7 days of 1NMPP1-induced inhibition of TrkB kinase activity ( $275 \pm 13 \mu\text{m}^2$ ) compared with CTL ( $268 \pm 21 \mu\text{m}^2$ , post hoc HSD test,  $P = 0.954$ ). Postsynaptic AChR density at individual diaphragm NMJs was estimated from the average Alexa Fluor 488-labeled  $\alpha$ -bungarotoxin. There were no significant differences in AChR density across the three experimental groups [ANOVA;  $F(2,15) = 3$ ;  $P = 0.107$ ].

Fig. 2. Representative confocal micrographs showing presynaptic terminals (labeled with synaptophysin) and motor end plates (labeled with  $\alpha$ -bungarotoxin) of neuromuscular junctions (NMJ) in the diaphragm muscle from adult *TrkB<sup>F616A</sup>* mice in CTL, INH, and REC experimental groups. On occasion, disruption of the motor axon and presynaptic terminal (asterisk) was evident in INMPP1-treated mice only. All confocal micrographs are maximum-projection images of confocal image stacks. Bar, 10  $\mu$ m.



An index of NMJ complexity was obtained from the relative planar area occupied by the motor end plate, as previously reported (45). Relative planar area was calculated using the motor end-plate and orthogonal areas (Fig. 3A) and reflects branching and fragmentation (reduced branching and fragmentation results in increased relative planar area). There were

significant differences in NMJ complexity across the three experimental groups [ANOVA;  $F(2,15) = 7$ ,  $P = 0.006$ ]. Following INMPP1-induced inhibition of TrkB kinase activity, the relative planar area increased significantly compared with CTL (Fig. 3B; post hoc HSD test,  $P = 0.005$ ). Thus INMPP1-induced inhibition of TrkB kinase activity reduced complexity (branching and fragmentation) of diaphragm muscle motor end plates without significant changes in 2D planar area.

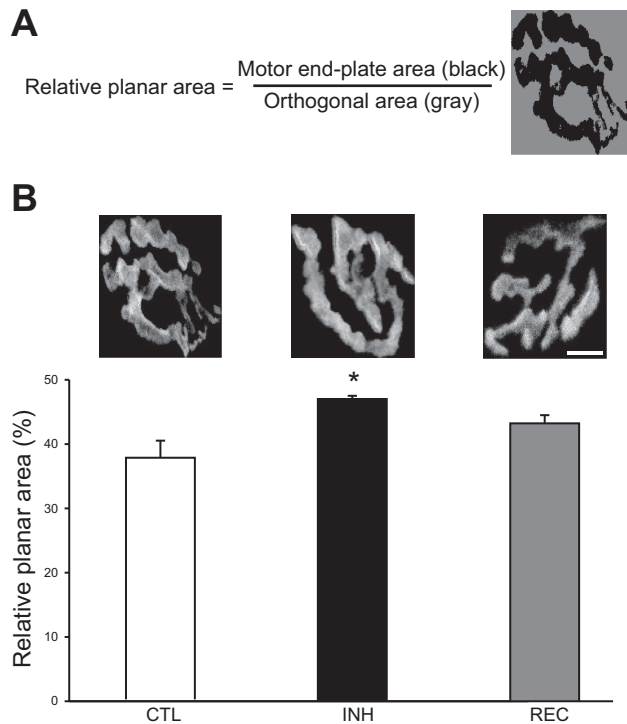


Fig. 3. Maximum-intensity projections of confocal image stacks were used to determine the relative planar area (an index of NMJ complexity reflecting branching and fragmentation) of diaphragm motor end plates in CTL, INH, and REC mice. *A*: a quantitative index of NMJ complexity was obtained from the ratio of the areas occupied by the motor end plate (after manual thresholding, black) and the area defined by the major orthogonal axes of each end plate (gray). *B*: relative planar area for *TrkB<sup>F616A</sup>* mice in CTL, INH, and REC groups with representative confocal images shown above each bar ( $n = 6$ /group). Inhibition of TrkB kinase activity with INMPP1 results in reduced complexity of motor end plates (ANOVA;  $P = 0.006$ ). \*Significantly different from CTL group (post hoc HSD test;  $P < 0.05$ ). Bar, 5  $\mu$ m.

3D analyses of NMJ morphology were used to examine changes in pre- and postsynaptic structures as a result of INMPP1-induced inhibition of TrkB kinase activity in *TrkB<sup>F616A</sup>* mice (Fig. 4). On average, 40 NMJs were analyzed from each animal with a total of 631 NMJs across the CTL, INH, and REC groups. Compared with CTL, the volume of motor end plates did not change significantly with INMPP1-induced inhibition of TrkB kinase activity (Fig. 5B; post hoc HSD test,  $P = 0.982$ ). No significant differences in the volume of presynaptic terminals were evident across the three experimental groups [Fig. 5A; ANOVA;  $F(2,13) = 1$ ,  $P = 0.345$ ]. However, there was a statistically significant difference in the fraction of the presynaptic terminal directly opposing the motor end plate across all groups [Fig. 4; ANOVA;  $F(2,13) = 8$ ,  $P = 0.007$ ]. Interestingly, the fraction of the presynaptic terminal volume directly opposing the motor end plate was greater in the INH group compared with CTL ( $68.1 \pm 4.1\%$  vs.  $49.0 \pm 5.8\%$ , respectively; post hoc HSD test,  $P = 0.017$ ). Increased 3D apposition (i.e., overlap) of pre- and postsynaptic structures is consistent with the reduced complexity evident in the 2D planar analyses of diaphragm motor end plates (Fig. 3).

*TrkB* kinase inhibition does not change quantal content in diaphragm NMJs. Electrophysiological measurements were conducted at individual diaphragm NMJs in CTL and INH groups (Fig. 6). Intracellular recordings did not detect differences in resting membrane potential across groups (CTL:  $-70.7 \pm 1.6$  mV; INH:  $-70.8 \pm 0.7$  mV;  $P = 0.99$ ). There were no differences in mEPP frequency (CTL:  $90 \pm 13$  min<sup>-1</sup>; INH:  $94 \pm 7$  min<sup>-1</sup>;  $P = 0.76$ ), but mEPP amplitude was greater at diaphragm NMJs of mice in the INH group compared with CTL (Table 2). The rise time was comparable across NMJs in both groups, suggesting that differences in mEPP

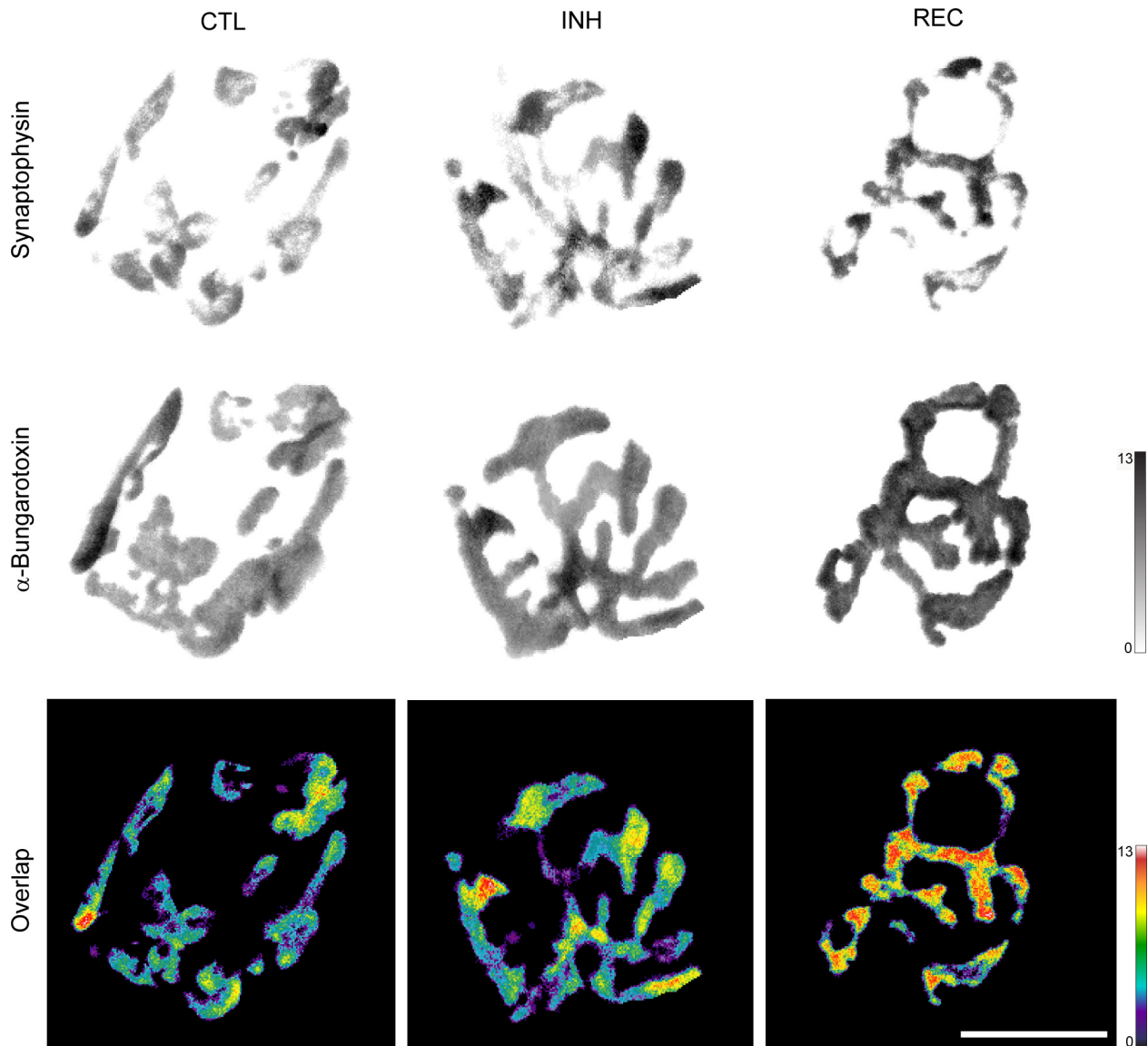


Fig. 4. Representative three-dimensional (3D) reconstructions of diaphragm muscle NMJs from *TrkB*<sup>F616A</sup> mice in CTL, INH, and REC groups. Presynaptic terminals (labeled with synaptophysin) and motor end plates (labeled with  $\alpha$ -bungarotoxin) show varying depth by grayscale intensity ( $\mu\text{m}$ , scale bar at right). The superimposed overlap representing the apposition of pre- and postsynaptic structures is shown in pseudocolor with depth shown by scale at right ( $\mu\text{m}$ ; red-white reflects greatest apposition). Notice that the presynaptic terminal volume directly opposing the motor end plate increased in the INH and REC groups compared with CTL (increased fraction of the NMJ in yellow-red colors). Bar, 10  $\mu\text{m}$ .

amplitude across groups are not related postsynaptic receptor kinetics (Fig. 6). To determine the quantal content released per stimulus, EPP amplitude was divided by mEPP amplitude after correction for nonlinear summation (31). Assuming all vesicles contribute equally to the EPP amplitude, the average initial quantal content for diaphragm NMJs in CTL and INH groups was not different ( $\sim 70$  quanta/stimulus;  $P = 0.86$ ).

**Recovery after TrkB kinase inhibition results in postsynaptic remodeling.** Following 7 days of recovery without the inhibitor 1NMPP1, the 2D planar area of diaphragm motor end plates increased ( $330 \pm 16 \mu\text{m}^2$ ), but this change was not significantly different compared with INH or CTL (post hoc HSD test,  $P = 0.091$  and  $P = 0.053$ , respectively). Motor end-plate complexity (branching and fragmentation) determined by the relative planar area was between values in the INH or CTL

groups but was not significantly different from either group (Fig. 3B; post hoc HSD test,  $P = 0.314$  and  $P = 0.090$ , respectively). Thus following 7 days of 1NMPP1 withdrawal there was only partial recovery of 1NMPP1-induced reduction in motor end-plate complexity.

Significant differences were observed in the volume of motor end plates across the three experimental groups [ANOVA;  $F(2,13) = 9$ ,  $P = 0.003$ ]. Of note, motor end-plate volume increased significantly following recovery from 1NMPP1-induced inhibition of TrkB kinase activity (Fig. 5B; post hoc HSD test,  $P = 0.007$  vs. INH and  $P = 0.007$  vs. CTL). Taken together, these findings suggest that motor end plates display increased gutter depth following recovery of TrkB kinase activity.

Presynaptically, there were no significant changes in terminal volume in the REC group compared with INH or CTL (Fig.

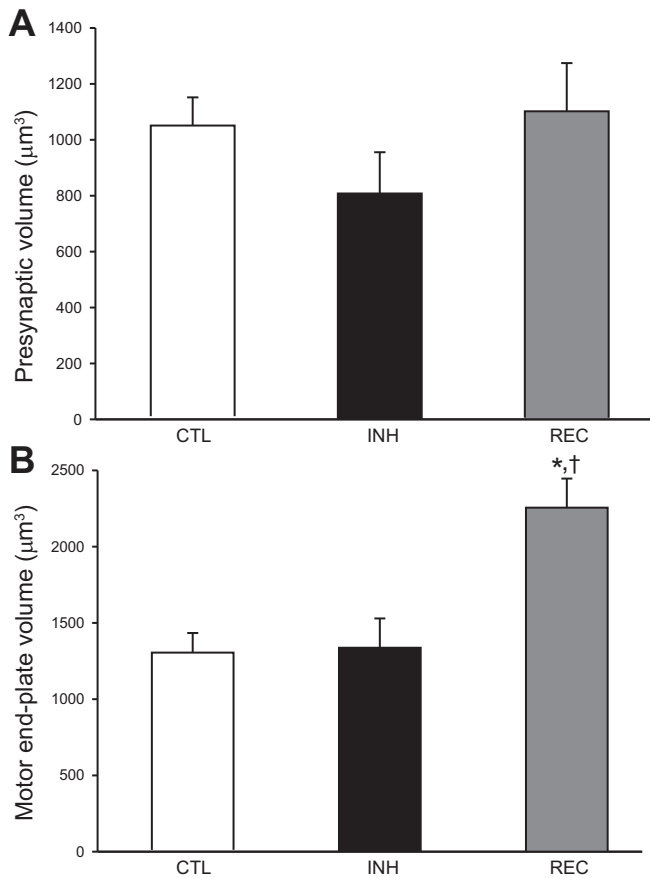


Fig. 5. Presynaptic and motor end-plate volume for diaphragm muscle NMJs from adult *TrkB<sup>F616A</sup>* mice in CTL, INH, and REC groups ( $n = 5-6/\text{group}$ ). *A*: the volume of the presynaptic terminal of diaphragm NMJs was not significantly different across experimental groups (ANOVA;  $P = 0.345$ ). *B*: the volume occupied by motor end plates did not change significantly with 1NMPP1-induced inhibition of TrkB kinase activity. Recovery significantly increased motor end-plate volume beyond INH and CTL levels. \*Significantly different from CTL group ( $P < 0.05$ ). †Significantly different from INH group ( $P < 0.05$ ). Data are means  $\pm$  SE.

5A; post hoc HSD test,  $P = 0.360$  and  $P = 0.958$ , respectively). Of note, the fraction of the presynaptic terminal volume directly opposing the motor end plate was greater in the REC group ( $71.0 \pm 4.4\%$ ) compared with CTL (post hoc HSD test,  $P = 0.009$ ) and not different compared with INH (post hoc HSD test,  $P = 0.880$ ). Thus increased apposition of pre- and postsynaptic structures following 1NMPP1-induced inhibition of TrkB kinase activity is still present following 7 days of recovery.

## DISCUSSION

Using a chemical-genetic approach that allows selective and reversible inhibition of TrkB kinase activity (6), we show that TrkB signaling is a critical determinant of functional and structural properties of NMJs in the adult mouse. Inhibition of TrkB kinase activity significantly impaired neuromuscular transmission. Quantal content assessed using electrophysiological recordings at individual diaphragm NMJs was not affected by inhibition of TrkB kinase activity, suggesting that changes in neuromuscular transmission reflect altered synaptic vesicle cycling. In agreement, there were no signs of denervation at the

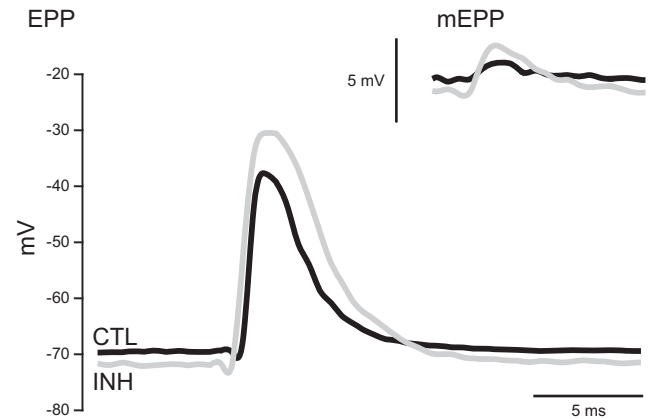


Fig. 6. Representative evoked end-plate potential (EPP) and miniature evoked end-plate potentials (mEPP; inset) tracings from *TrkB<sup>F616A</sup>* mice in CTL (black) and INH (gray) groups. Note different voltage scales for the 2 sets of tracings.

NMJ. Furthermore, complexity of motor end plates was reduced, and apposition of presynaptic terminals to motor end plates at diaphragm NMJs increased, indicating that these morphological changes are not likely responsible for the functional changes associated with inhibition of TrkB kinase activity. Recovery of TrkB kinase activity was accompanied by a restoration of neuromuscular transmission and remodeling of motor end plates (consistent with increased gutter depth) without substantial restoration of motor end-plate complexity or apposition of pre- and postsynaptic structures. Taken together, these results highlight the importance of TrkB kinase activity in the maintenance of functional and structural properties at adult NMJs in vivo, and seemingly discordant structure-function relationships at remodeling NMJs (45).

*TrkB kinase activity modulates neuromuscular transmission.* Previous studies using short-term application of TrkB agonists at the NMJ support the importance of TrkB kinase activity in enhancing synaptic transmission at the adult NMJ (14, 25, 30). For instance, the TrkB ligands BDNF, NT-4, and 7,8-dihydroxyflavone significantly improved neuromuscular transmission at rodent diaphragm NMJs in vitro (25, 30). These findings suggest a role of TrkB kinase activity in maintaining neuromuscular transmission during repetitive stimulation. In agreement, neuromuscular transmission was impaired following in vitro treatment with K252a, a TrkB kinase receptor inhibitor, in rat diaphragm muscle-phrenic nerve preparations (30). TrkB kinase activity is necessary for TrkB ligand effects

Table 2. Electrophysiological characteristics of diaphragm neuromuscular junctions (NMJ) in *TrkB<sup>F616A</sup>* mice

	mEPP Amplitude, mV	EPP Amplitude, mV	Quantal Content
Control <i>TrkB<sup>F616A</sup></i> (CTL)	1.0 $\pm$ 0.2	33.0 $\pm$ 0.5	66.6 $\pm$ 6.4
1NMPP1-Inhibited (INH)	1.5 $\pm$ 0.1*	40.9 $\pm$ 1.3*	68.0 $\pm$ 2.8

Data are presented as means  $\pm$  SE. Measurements were obtained from  $n = 5$  (total 22 NMJs) and  $n = 4$  (total 25 NMJs) *TrkB<sup>F616A</sup>* mice in the CTL and INH groups, respectively. mEPP and EPP, miniature end-plate potential and end-plate potential, respectively. See Fig. 6 for representative tracings. \*Significantly different from CTL group [mEPP:  $t(4.9)$ ,  $P = 0.002$ ; EPP:  $t(5.6)$ ,  $P = 0.005$ ].

on neuromuscular transmission. Indeed, concomitant treatment in vitro with 7,8-dihydroxyflavone and the TrkB kinase inhibitor 1NMPP1 in preparations from *TrkB<sup>F616A</sup>* mice resulted in impaired neuromuscular transmission compared with control (25). Quantal content at individual diaphragm NMJs was not affected by inhibition of TrkB kinase activity. In a previous study in the levator auris longus of adult mice (14), in vitro treatment with the TrkB fusion protein TrkB-IgG did not affect EPP amplitude. Importantly, the current study examined neuromuscular transmission, using a global measure of transmission failure and electrophysiological recordings at individual diaphragm NMJs. These results demonstrate significantly impaired neuromuscular transmission following 7 days of in vivo 1NMPP1 treatment in *TrkB<sup>F616A</sup>* mice. Overall, these results suggest that TrkB kinase activity plays an important role in maintenance of neuromuscular function at adult NMJs.

In other synapses, BDNF signaling via TrkB receptors also regulates cholinergic neurotransmission. In the hippocampus, BDNF enhances acetylcholine release from septal cholinergic neurons (20) and increases inhibitory cholinergic currents (5). In postganglionic sympathetic neurons innervating the heart, BDNF increases acetylcholine release (55), increasing miniature excitatory postsynaptic current amplitude while not altering their frequency (24). In intestinal (1) and airway (36) smooth muscles, BDNF signaling via TrkB enhances cholinergic agonist-induced muscle contraction.

Neurotrophin signaling via TrkB receptors is relevant to the maintenance of function and structure at the NMJ, but not muscle fibers, even though muscle fibers also may express TrkB receptors (29, 44). Indeed, isometric contractile and fatigue properties in the diaphragm muscle are consistently unaffected by TrkB receptor activation induced by BDNF (30), inhibition resulting from in vitro 1NMPP1 (25), as well as following inhibition and recovery of TrkB kinase activity following in vivo treatment (present study). It is noteworthy that impaired neuromuscular transmission was evident in diaphragm muscle-phrenic nerve preparations from 1NMPP1-treated *TrkB<sup>F616A</sup>* mice even though 1NMPP1 was only administered orally (in vivo) and was absent from the bath during in vitro testing of neuromuscular transmission failure. In a previous study (25), administration of 1NMPP1 in vitro acutely impaired neuromuscular transmission in preparations from *TrkB<sup>F616A</sup>* mice ( $52.8 \pm 3.4\%$ ). Thus 1NMPP1 was omitted during in vitro testing in the present study. Of note, the impairment in neuromuscular transmission was similar following in vitro treatment and 7 days of oral 1NMPP1 treatment ( $58.9 \pm 3.7\%$ ), suggesting that impairments in neuromuscular transmission resulting from inhibition of TrkB kinase activity do not depend on the morphological changes observed at diaphragm NMJs.

*TrkB kinase activity is necessary to maintain motor end-plate integrity.* Inhibiting TrkB kinase activity (with 1NMPP1) reduced overall postsynaptic branching and fragmentation in the diaphragm muscle of *TrkB<sup>F616A</sup>* mice. Importantly, these modest morphological changes at diaphragm NMJs take place in a time frame where substantial functional and morphological changes were shown in models of altered synaptic activity (27, 28, 38, 48, 49). The reduced complexity (branching and fragmentation) of motor end plates and increased apposition of pre- and postsynaptic structures following treatment with 1NMPP1 for 7 days in *TrkB<sup>F616A</sup>* mice are more consistent with im-

proved (rather than impaired) neuromuscular transmission. In particular, reduced branching and fragmentation can be expected to reduce the likelihood of branch-point failure (47). Increased apposition of pre- and postsynaptic structures occurs in conditions where neuromuscular transmission improves (42). In addition, the increased apposition of nerve terminals and motor end plates at type I fibers compared with type IIx and/or IIb is associated with differences in neuromuscular transmission, safety factor, and synaptic vesicle release (9, 37, 43).

Using genetic knockdown models, Gonzalez et al. (15) and Kulakowski et al. (22) showed that TrkB expression is important for NMJ structure. In adult *TrkB<sup>+/-</sup>* mice, NMJs displayed an increased number of AChR clusters at motor end plates in both the sternomastoid (15) and soleus muscles (22), suggesting disassembly of postsynaptic structures in muscles with reduced TrkB expression throughout their lifespan. Similar postsynaptic disassembly was also reported with reduced TrkB signaling in a mouse model of severe combined immunodeficiency in which *TrkB.t1* was overexpressed by adenovirus delivery to the surface of the sternomastoid muscle (15) and in a NT-4 knockout mouse model (2). In contrast, inhibiting TrkB kinase activity (with 1NMPP1) was associated with modest morphological changes at diaphragm NMJs. Thus it is possible that chronically reduced neurotrophin or TrkB expression may result in developmental alterations in motor end-plate morphology that are evident in the adult but that do not reflect and are independent of TrkB kinase activity in intact adult NMJs. Differences in neurotrophin effects across motor end plates at different fiber types may also contribute to reported differences across studies. The sternomastoid muscle in mice predominantly comprises type IIb and/or IIx fibers (~85%) (16). In contrast, the diaphragm and soleus muscles are more mixed in fiber type composition and comprise few type IIb fibers. In mice, the diaphragm muscle comprises ~10% type I, 50% type IIa, and 38% type IIx fibers (45), and the soleus muscle contains ~30% type I, 50% type IIa, and 12% type IIx fibers (4, 51). Thus it is possible that differences in the effect of TrkB kinase activity on motor end-plate structure may be present across fiber types. Of note, diaphragm NMJs cannot be fiber type-identified in the mouse based on morphological measurements (45), although there are reliable motor end-plate characteristics that permit fiber typing in the rat (9, 26, 27, 37, 49). Regardless, there was no evidence of a bimodal distribution for any of the motor end-plate measurements across experimental groups (Shapiro-Wilk goodness-of-fit test for a binomial distribution,  $P > 0.05$  in each case), suggesting that inhibition (and recovery) of TrkB kinase activity exert similar effects across all fiber types in the adult mouse diaphragm muscle.

A systematic, blinded and unbiased approach was used to assess motor end-plate complexity in the present study that was based on our previous report (45). This measurement of complexity considers the relative planar area occupied by the motor end plate. Other studies have used manual counts of AChR clusters at each motor end plate in assessments of the role of neurotrophins or Trk receptors at the NMJ (2, 8, 15, 22). Of note, the number of AChR clusters does not influence measurements of relative planar area, particularly if the orthogonal area delimited by the major axes of a motor end plate is reduced or unchanged (as was the case in the diaphragm muscle). Thus reduced complexity of motor end plates follow-

ing inhibition of TrkB kinase activity is not necessarily inconsistent with an increased number of AChR clusters as reported by Gonzalez et al. (15) and Kulakowski et al. (22). Indeed, the overall motor end-plate area was reduced in the sternomastoid muscle of *TrkB*<sup>+/-</sup> mice compared with *TrkB*<sup>+/+</sup> mice (15), suggesting that the relative planar area did not change. In contrast, motor end plates were larger in the soleus muscle (22), and thus it is not possible to ascertain a possible effect on the complexity measure utilized in the present study. Regardless, motor end-plate disassembly characterized by increased numbers of AChR clusters was not a prominent feature following 7 days of inhibition of TrkB kinase activity with 1NMPP1 in *TrkB*<sup>F616A</sup> mice.

*TrkB kinase activity and presynaptic terminal integrity.* Previous studies have not consistently examined presynaptic adaptations to reduced TrkB expression and/or signaling in genetic knockdown models (2, 8, 15, 22). Compared with *TrkB*<sup>+/+</sup> mice, there was no significant difference in pre- and postsynaptic terminal overlap in the soleus muscle of *TrkB*<sup>+/-</sup> mice (22). These measurements were based on 2D maximum-intensity projections and thus may not adequately account for the size and apposition of pre- and postsynaptic structures. Indeed, 2D measurements of apposition overestimate apposition of pre- and postsynaptic structures by up to 40%. In the present study, 3D analyses of NMJ morphology showed that inhibition of TrkB kinase activity significantly increased the fraction of the presynaptic terminal volume in apposition with the motor end plate. The extent of apposition has been shown to vary by fiber type using 2D projections in rats (35, 38), such that variance due to fiber types may also be a factor in 3D measurements of apposition. However, detailed 3D information of diaphragm NMJ structure in mice is not available at present.

Oral 1NMPP1 treatment clearly may exert effects at other sites distinct from the NMJ itself. For instance, TrkB kinase activity at the neuronal cell body is necessary for dendritic BDNF effects on gene expression in cultured embryonic rat cortical neurons (7). Thus TrkB kinase activity at phrenic motor neurons (whether at their cell body or presynaptic terminal) may contribute to the maintenance of functional and structural properties at adult diaphragm NMJs. Indirect effects (e.g., via Schwann cells and axon myelination) may also be possible (34).

*Functional and structural properties at the NMJ following recovery from inhibition of TrkB kinase activity.* The reversibility of 1NMPP1 effects on TrkB kinase activity following pharmacological withdrawal permits examination of recovery of TrkB kinase activity in vivo. Thus this model provides unique insight into the dynamic regulation of NMJ integrity both pre- and postsynaptically. Despite modest restoration of morphological changes following withdrawal of 1NMPP1 and recovery of TrkB kinase activity, the impairment in neuromuscular transmission was completely reversible. These results highlight complex structure-function relationships at remodeling NMJs.

Previous studies have used genetic deletion models to examine changes in TrkB activity at the NMJ. For instance, genetic deletion of the truncated TrkB.t1 receptor isoform will likely increase TrkB signaling, given that kinase activity depends on full-length, not truncated TrkB receptors (17). In this sense, results in the *TrkB.t1*<sup>-/-</sup> mouse (8) should resemble

those seen in *TrkB*<sup>F616A</sup> mice following recovery after inhibition of TrkB kinase activity. Indeed, genetic deletion of TrkB.t1 resulted in a modest expansion in the planar area of motor end plates (8). Although the 2D planar area of diaphragm NMJs increased slightly with recovery of TrkB kinase activity following withdrawal of 1NMPP1 in *TrkB*<sup>F616A</sup> mice, the observed remodeling of motor end plates suggests an increase in gutter depth in the recovered group given the increase in motor end-plate volume. Increased gutter depth would be expected to improve synaptic transmission by increasing the number of voltage-gated Na<sup>+</sup> channels in the vicinity of AChR (9, 43), increasing the safety factor (54). Electrophysiological measurements (perijunctional resting membrane potential, mEPP frequency, and mEPP rise time) following inhibition of TrkB kinase activity suggest that postsynaptic receptor kinetics do not contribute to the impairment in neuromuscular transmission. In agreement, changes in motor end-plate complexity induced by inhibition of TrkB kinase activity were not restored after recovery, yet neuromuscular transmission was restored. Furthermore, inhibition of TrkB kinase activity resulted in no alteration of quantal content at individual diaphragm NMJs. The small changes in mEPP amplitude are consistent with the increased apposition of pre- and postsynaptic structures following inhibition of TrkB kinase activity. Increased EPP amplitude is consistent with the reduced complexity of motor end plates. Effects on AChR density are unlikely to have contributed to the measured electrophysiological changes since measurements of  $\alpha$ -bungarotoxin-based fluorescence did not change across experimental groups. The lack of changes in presynaptic terminal volume does not suggest changes in total number of synaptic vesicles as contributing to altered neuromuscular transmission. Taken together, changes in synaptic vesicle cycling as a result of altered expression of synaptic vesicle proteins and/or altered vesicle release kinetics are likely responsible for the reversible impairment in neuromuscular transmission following inhibition and recovery of TrkB kinase activity.

*Conclusions.* The complementary electrophysiological and morphological studies using a chemical-genetic approach to reversibly inhibit TrkB kinase activity in vivo support the importance of neurotrophin signaling via TrkB kinase activity for regulation of neurotransmitter release in the short term and for maintenance of synaptic function and structural integrity at adult rodent NMJs in the long term. Furthermore, the results of the present study suggest a possible therapeutic role for TrkB agonists in diseases associated with impaired neuromuscular transmission, including neuromuscular disorders. Disruption of trophic interactions at the NMJ may also contribute to a number of conditions throughout the lifespan and may be important for repair and regeneration following injury. The role of structural adaptations at the NMJ in defining functional properties is less clear, suggesting that future investigations not restrict the study of neuromuscular adaptations to morphological analyses but include functional evaluations that consider both global and specific effects at individual synapses. The reversible impairment of NMJ function following inhibition and recovery of TrkB kinase activity likely reflects deficits in the release of synaptic vesicles rather than apposition of pre- and postsynaptic structures or NMJ complexity.

## ACKNOWLEDGMENTS

We thank Y.-H. Fang for technical assistance with the performance of immunohistochemical studies. Dr. D. D. Ginty (Johns Hopkins University) kindly provided the original breeder pair of *TrkB<sup>F616A</sup>* knock-in mice.

## GRANTS

This work was supported by National Institutes of Health Grants HL-096750, HL-105355, and AG-044615 and the Mayo Clinic.

## DISCLOSURES

No conflicts of interest, financial or otherwise, are declared by the author(s).

## AUTHOR CONTRIBUTIONS

Author contributions: C.B.M. and G.C.S. conception and design of research; C.B.M., J.M.S., D.C.S., and L.G.E. performed experiments; C.B.M., J.M.S., D.C.S., L.G.E., S.M.G., and G.C.S. analyzed data; C.B.M., J.M.S., D.C.S., L.G.E., S.M.G., and G.C.S. interpreted results of experiments; C.B.M., J.M.S., D.C.S., and L.G.E. prepared figures; C.B.M., J.M.S., D.C.S., and S.M.G. drafted manuscript; C.B.M., J.M.S., D.C.S., L.G.E., S.M.G., C.Z., K.M.S., and G.C.S. edited and revised manuscript; C.B.M., J.M.S., D.C.S., L.G.E., S.M.G., C.Z., K.M.S., and G.C.S. approved final version of manuscript.

## REFERENCES

- Al-Qudah M, Anderson CD, Mahavadi S, Bradley ZL, Akbarali HI, Murthy KS, Grider JR. Brain-derived neurotrophic factor enhances cholinergic contraction of longitudinal muscle of rabbit intestine via activation of phospholipase C. *Am J Physiol Gastrointest Liver Physiol* 306: G328–G337, 2014.
- Belluardo N, Westerblad H, Mudo G, Casabona A, Bruton J, Caniglia G, Pastoris O, Grassi F, Ibanez CF. Neuromuscular junction disassembly and muscle fatigue in mice lacking neurotrophin-4. *Mol Cell Neurosci* 18: 56–67, 2001.
- Benjamin KR, Zhang C, Shokat KM, Herskowitz I. Control of landmark events in meiosis by the CDK Cdc28 and the meiosis-specific kinase Ime2. *Genes Dev* 17: 1524–1539, 2003.
- Bloemberg D, Quadrilatero J. Rapid determination of myosin heavy chain expression in rat, mouse, and human skeletal muscle using multi-color immunofluorescence analysis. *PLoS One* 7: e35273, 2012.
- Cabezas C, Buno W. BDNF is required for the induction of a presynaptic component of the functional conversion of silent synapses. *Hippocampus* 21: 374–385, 2011.
- Chen X, Ye H, Kuruvilla R, Ramanan N, Scangos KW, Zhang C, Johnson NM, England PM, Shokat KM, Ginty DD. A chemical-genetic approach to studying neurotrophin signaling. *Neuron* 46: 13–21, 2005.
- Cohen MS, Bas Orth C, Kim HJ, Jeon NL, Jaffrey SR. Neurotrophin-mediated dendrite-to-nucleus signaling revealed by microfluidic compartmentalization of dendrites. *Proc Natl Acad Sci USA* 108: 11246–11251, 2011.
- Dorsey SG, Lovering RM, Renn CL, Leitch CC, Liu X, Tallon LJ, Sadzewicz LD, Pratap A, Ott S, Sengamalay N, Jones KM, Barrick C, Fulgenzi G, Becker J, Voelker K, Talmadge R, Harvey BK, Wyatt RM, Vernon-Pitts E, Zhang C, Shokat K, Fraser-Liggett C, Balice-Gordon RJ, Tessarollo L, Ward CW. Genetic deletion of *trkB.T1* increases neuromuscular function. *Am J Physiol Cell Physiol* 302: C141–C153, 2012.
- Ermilov LG, Mantilla CB, Rowley KL, Sieck GC. Safety factor for neuromuscular transmission at type-identified diaphragm fibers. *Muscle Nerve* 35: 800–803, 2007.
- Ermilov LG, Pulido JN, Atchison FW, Zhan WZ, Ereth MH, Sieck GC, Mantilla CB. Impairment of diaphragm muscle force and neuromuscular transmission after normothermic cardiopulmonary bypass: effect of low dose inhaled CO. *Am J Physiol Regul Integr Comp Physiol* 298: R784–R789, 2010.
- Fournier M, Alula M, Sieck GC. Neuromuscular transmission failure during postnatal development. *Neurosci Lett* 125: 34–36, 1991.
- Funakoshi H, Belluardo N, Arenasa E, Yamamoto Y, Casabona A, Persson H, Ibanez CF. Muscle-derived neurotrophin-4 as an activity-dependent trophic signal for adult motor neurons. *Science* 268: 1495–1499, 1995.
- Garcia N, Santafe MM, Tomas M, Lanuza MA, Besalduch N, Tomas J. Involvement of brain-derived neurotrophic factor (BDNF) in the functional elimination of synaptic contacts at polyinnervated neuromuscular synapses during development. *J Neurosci Res* 88: 1406–1419, 2010.
- Garcia N, Tomas M, Santafe MM, Besalduch N, Lanuza MA, Tomas J. The interaction between tropomyosin-related kinase B receptors and presynaptic muscarinic receptors modulates transmitter release in adult rodent motor nerve terminals. *J Neurosci* 30: 16514–16522, 2010.
- Gonzalez M, Ruggiero FP, Chang Q, Shi YJ, Rich MM, Kraner S, Balice-Gordon RJ. Disruption of TrkB-mediated signaling induces disassembly of postsynaptic receptor clusters at neuromuscular junctions. *Neuron* 24: 567–583, 1999.
- Guido AN, Campos GE, Neto HS, Marques MJ, Minatel E. Fiber type composition of the sternomastoid and diaphragm muscles of dystrophin-deficient mdx mice. *Anat Rec (Hoboken)* 293: 1722–1728, 2010.
- Huang EJ, Reichardt LF. Trk receptors: roles in neuronal signal transduction. *Annu Rev Biochem* 72: 609–642, 2003.
- Johnson BD, Sieck GC. Differential susceptibility of diaphragm muscle fibers to neuromuscular transmission failure. *J Appl Physiol* 75: 341–348, 1993.
- Knaus P, Betz H. Mapping of a dominant immunogenic region of synaptophysin, a major membrane protein of synaptic vesicles. *FEBS Lett* 261: 358–360, 1990.
- Knipper M, da Penha Berzaghi M, Blochl A, Breer H, Thoenen H, Lindholm D. Positive feedback between acetylcholine and the neurotrophins nerve growth factor and brain-derived neurotrophic factor in the rat hippocampus. *Eur J Neurosci* 6: 668–671, 1994.
- Kuei JH, Shadmehr R, Sieck GC. Relative contribution of neurotransmission failure to diaphragm fatigue. *J Appl Physiol* 68: 174–180, 1990.
- Kulakowski SA, Parker SD, Personius KE. Reduced TrkB expression results in precocious age-like changes in neuromuscular structure, neurotransmission, and muscle function. *J Appl Physiol* 111: 844–852, 2011.
- Lohof AM, Ip NY, Poo MM. Potentiation of developing neuromuscular synapses by the neurotrophins NT-3 and BDNF. *Nature* 363: 350–353, 1993.
- Luther JA, Enes J, Birren SJ. Neurotrophins regulate cholinergic synaptic transmission in cultured rat sympathetic neurons through a p75-dependent mechanism. *J Neurophysiol* 109: 485–496, 2013.
- Mantilla CB, Ermilov LG. The novel TrkB receptor agonist 7,8-dihydroxyflavone enhances neuromuscular transmission. *Muscle Nerve* 45: 274–276, 2012.
- Mantilla CB, Rowley KL, Fahim MA, Zhan WZ, Sieck GC. Synaptic vesicle cycling at type-identified diaphragm neuromuscular junctions. *Muscle Nerve* 30: 774–783, 2004.
- Mantilla CB, Rowley KL, Zhan WZ, Fahim MA, Sieck GC. Synaptic vesicle pools at diaphragm neuromuscular junctions vary with motoneuron soma, not axon terminal, inactivity. *Neuroscience* 146: 178–189, 2007.
- Mantilla CB, Sieck GC. Neuromuscular adaptations to respiratory muscle inactivity. *Respir Physiol Neurobiol* 169: 133–140, 2009.
- Mantilla CB, Sieck GC. Trophic factor expression in phrenic motor neurons. *Respir Physiol Neurobiol* 164: 252–262, 2008.
- Mantilla CB, Zhan WZ, Sieck GC. Neurotrophins improve neuromuscular transmission in the adult rat diaphragm. *Muscle Nerve* 29: 381–386, 2004.
- McLachlan EM, Martin AR. Non-linear summation of end-plate potentials in the frog and mouse. *J Physiol* 311: 307–324, 1981.
- Miyata H, Zhan WZ, Prakash YS, Sieck GC. Influence of myoneural interactions on contractile properties of rat diaphragm. *Jpn J Exerc Physiol* 2: 167–176, 1995.
- Miyata H, Zhan WZ, Prakash YS, Sieck GC. Myoneural interactions affect diaphragm muscle adaptations to inactivity. *J Appl Physiol* 79: 1640–1649, 1995.
- Ng BK, Chen L, Mandemakers W, Cosgaya JM, Chan JR. Anterograde transport and secretion of brain-derived neurotrophic factor along sensory axons promote Schwann cell myelination. *J Neurosci* 27: 7597–7603, 2007.
- Prakash YS, Gosselin LE, Zhan WZ, Sieck GC. Alterations of diaphragm neuromuscular junctions with hypothyroidism. *J Appl Physiol* 81: 1240–1248, 1996.
- Prakash YS, Iyanoye A, Ay B, Mantilla CB, Pabelick CM. Neurotrophin effects on intracellular Ca<sup>2+</sup> and force in airway smooth muscle. *Am J Physiol Lung Cell Mol Physiol* 291: L447–L456, 2006.

37. **Prakash YS, Miller SM, Huang M, Sieck GC.** Morphology of diaphragm neuromuscular junctions on different fibre types. *J Neurocytol* 25: 88–100, 1996.
38. **Prakash YS, Miyata H, Zhan WZ, Sieck GC.** Inactivity-induced remodeling of neuromuscular junctions in rat diaphragmatic muscle. *Muscle Nerve* 22: 307–319, 1999.
39. **Prakash YS, Sieck GC.** Age-related remodeling of neuromuscular junctions on type-identified diaphragm fibers. *Muscle Nerve* 21: 887–895, 1998.
40. **Prakash YS, Smithson KG, Sieck GC.** Application of the Cavalieri principle in volume estimation using laser confocal microscopy. *Neuroimage* 1: 325–333, 1994.
41. **Prakash YS, Smithson KG, Sieck GC.** Measurements of motoneuron somal volumes using laser confocal microscopy: comparisons with shape-based stereological estimations. *Neuroimage* 1: 95–107, 1993.
42. **Prakash YS, Zhan WZ, Miyata H, Sieck GC.** Adaptations of diaphragm neuromuscular junction following inactivity. *Acta Anat (Basel)* 154: 147–161, 1995.
43. **Rowley KL, Mantilla CB, Ermilov LG, Sieck GC.** Synaptic vesicle distribution and release at rat diaphragm neuromuscular junctions. *J Neurophysiol* 98: 478–487, 2007.
44. **Sakuma K, Watanabe K, Sano M, Uramoto I, Nakano H, Li YJ, Kaneda S, Sorimachi Y, Yoshimoto K, Yasuhara M, Totsuka T.** A possible role for BDNF, NT-4 and TrkB in the spinal cord and muscle of rat subjected to mechanical overload, bupivacaine injection and axotomy. *Brain Res* 907: 1–19, 2001.
45. **Sieck DC, Zhan WZ, Fang YH, Ermilov LG, Sieck GC, Mantilla CB.** Structure-activity relationships in rodent diaphragm muscle fibers vs. neuromuscular junctions. *Respir Physiol Neurobiol* 180: 88–96, 2012.
46. **Sieck GC, Mantilla CB, Prakash YS.** Volume measurements in confocal microscopy. *Methods Enzymol* 307: 296–315, 1999.
47. **Sieck GC, Prakash YS.** Fatigue at the neuromuscular junction. Branch point vs. presynaptic vs. postsynaptic mechanisms. *Adv Exp Med Biol* 384: 83–100, 1995.
48. **Sieck GC, Prakash YS.** Morphological adaptations of neuromuscular junctions depend on fiber type. *Can J Appl Physiol* 22: 197–230, 1997.
49. **Sieck GC, Van Balkom RH, Prakash YS, Zhan WZ, Dekhuijzen PN.** Corticosteroid effects on diaphragm neuromuscular junctions. *J Appl Physiol* 86: 114–122, 1999.
50. **Snider WD.** Functions of the neurotrophins during nervous system development: what the knockouts are teaching us. *Cell* 77: 627–638, 1994.
51. **Totsuka Y, Nagao Y, Horii T, Yonekawa H, Imai H, Hatta H, Izaike Y, Tokunaga T, Atomi Y.** Physical performance and soleus muscle fiber composition in wild-derived and laboratory inbred mouse strains. *J Appl Physiol* 95: 720–727, 2003.
52. **Wang XH, Poo MM.** Potentiation of developing synapses by postsynaptic release of neurotrophin-4. *Neuron* 19: 825–835, 1997.
53. **Wiedenmann B, Franke WW.** Identification and localization of synaptophysin, an integral membrane glycoprotein of Mr 38,000 characteristic of presynaptic vesicles. *Cell* 41: 1017–1028, 1985.
54. **Wood SJ, Slater CR.** The contribution of postsynaptic folds to the safety factor for neuromuscular transmission in rat fast- and slow-twitch muscles. *J Physiol* 500: 165–176, 1997.
55. **Yang B, Slonimsky JD, Birren SJ.** A rapid switch in sympathetic neurotransmitter release properties mediated by the p75 receptor. *Nat Neurosci* 5: 539–545, 2002.

